Original Research

The Effect of Rake Angle and Cutting Edge Radius on the Orthogonal Cutting Process of Ti6Al4V Alloy

Mohammed Mustafa [1], Salman Pervaiz [2, *], Ibrahim Deiab [1]

1. Advanced Manufacturing Lab (AML), School of Engineering, University of Guelph, Canada; E-Mails: mmusta05@uoguelph.ca; ideiab@uoguelph.ca
2. Mechanical and Industrial Engineering Department, Rochester Institute of Technology Dubai, United Arab Emirates; E-Mail: sxpcad@rit.edu

* **Correspondence:** Salman Pervaiz; E-Mail: sxpcad@rit.edu

Abstract

This paper investigates the effect of rake angle, α, cutting edge radius, r, and feed rate, f, on the cutting force and cutting zone temperature during orthogonal dry cutting of Ti6Al4V. A numerical model representative of the 2D orthogonal cutting process is developed using ABAQUS/Explicit software. Johnson-Cook, (JC) constitutive material model is used to describe material plasticity. JC damage model and energy-based fracture criterion are used to describe damage initiation and evolution. Using Minitab-19 software, Taguchi L9 orthogonal array (3 × 3) is implemented to plan simulation trails. Assuming a constant cutting speed of 500 mm/min, three levels for each factor are considered α (-5°, 0°, 5°), r (0.02, 0.04, 0.06 mm) and f (0.1, 0.2, 0.3 mm). The cutting force and cutting zone temperature are analyzed using ANOVA. Based on a 90% Confidence Interval (90% CI), the results show that only feed rate significantly affects the cutting force. However, rake angle, cutting edge radius, and feed rate do not substantially affect cutting zone temperature.

Keywords

Ti6Al4V; orthogonal cutting; finite element; Taguchi; ANOVA

1. Introduction

Ti6Al4V is one of the most commonly used titanium alloys [1] due to its superior mechanical and physical properties, such as high strength-to-density ratio, high fatigue and corrosion resistance, and good biocompatibility [2-4]. It is used for many applications in various fields, including aerospace, biomedical, nuclear, and automotive [4-7]. However, titanium alloys, including Ti6Al4V, are considered difficult-to-cut materials due to their low thermal conductivity, high strain hardening, hot temperature hardness, and high reactivity [2-4]. Low thermal conductivity restricts heat transfer from the cutting zone and leads to temperature rise during machining [5]. According to Zhen-Bin and Komanduri [8], this leads to the formation of serrated chips even at low cutting speed. This effect is more severe at high cutting speeds due to adiabatic shear banding in the primary shear zone [9].

Different techniques are used to overcome difficulties in machining Ti6Al4V. These include unconventional machining [10, 11], heat-induced machining [12], vibration-assisted machining [13], ultrasonically assisted machining [14], and hard turning and grinding [15]. However, conventional machining is the most common process in manufacturing titanium parts [2] as it can produce parts with high surface quality, high dimensional accuracy, high aspect ratio, and high fatigue strength with relativity low cost.

Many studies investigated conventional machining of Ti6Al4V to improve product surface integrity [16], improve cutting tool life [17], increase process efficiency, and reduce cutting forces and power consumption [18].

Different methodologies were used to study conventional machining processes of Ti6Al4V, including analytical, numerical, experimental, and statistical (DOE). In this study, a numerical model of 2D orthogonal dry machining of Ti6Al4V is created and used to study the effect of rake angle, cutting edge radius, and feed rate on cutting force and cutting zone temperature. In addition to lower cost, numerical simulation provides a means to determine parameters that are very difficult to measure physically, such as cutting zone temperature.

Taguchi L9 orthogonal array is used to plane the simulation trails. The Taguchi method is advantageous as it requires fewer simulation trials than a complete factorial design. For three factors with three levels each, 9 trials are necessary per Taguchi L9 (3 × 3), while 27 (3³) trials are required if the complete factorial design is used. Results of the numerical simulations are analyzed using ANOVA to study the effect of rake angle, cutting edge radius, and feed rate on both cutting force and cutting zone temperature.

As per Hall et al. [19], a limited number of numerical studies have been conducted to investigate the effect of cutting tool geometries on the machining process. As part of their study, Hall et al. [19] investigated the effect of rack angle on the cutting force. Two levels of rack angle were considered 12° and 14°. They found that rack angle has a statistically significant effect on the cutting force. Increasing rack angle results in decreasing cutting forces. However, they have reported that their computational results have discrepancies and differ from experimental results. Li et al. [20] studied the effect of rack angle on chip formation and the adiabatic shear banding process. Seven levels of rack angle were considered -15°, -10°, -5°, 0°, 5°, 10°, 15°. As part of their study, the effect of rake angle on the Hight Temperature Zone (HTZ) temperature was investigated. They found that

increasing rack angle decreases the temperature of HTZ. Pervaiz et al. [21] studied the effect of rack angle on cutting energy and cutting force, and they used three levels of rack angle in their analysis -10°, 0°, and 10°. They reported that decreasing rack angle results in increasing cutting force. Selvakumar S and Raj. D [22] investigated the effect of cutting-edge radius on cutting and thrust forces. They found that increasing cutting-edge radius increases both cutting and thrust forces. However, the thrust force is more sensitive to the cutting-edge radius. Chen et al. [23] and Chen et al. [24] studied the effect of cutting-edge radius on the cutting and thrust force under different cooling/lubricating strategies. Similar results were found as per [22]. This study investigates the effect of rake angle, cutting edge radius, and feed rate on the cutting force and cutting zone temperature based on numerical and statistical analysis.

2. Numerical Modelling

2.1 Geometry, Meshing, and Boundary Conditions

This study created a 2D orthogonal cutting model using the ABAQUS/CAE software. Explicit Lagrangian formulation is implemented assuming plane strain conditions. Figure 1 describes the geometry and boundary conditions of the model.
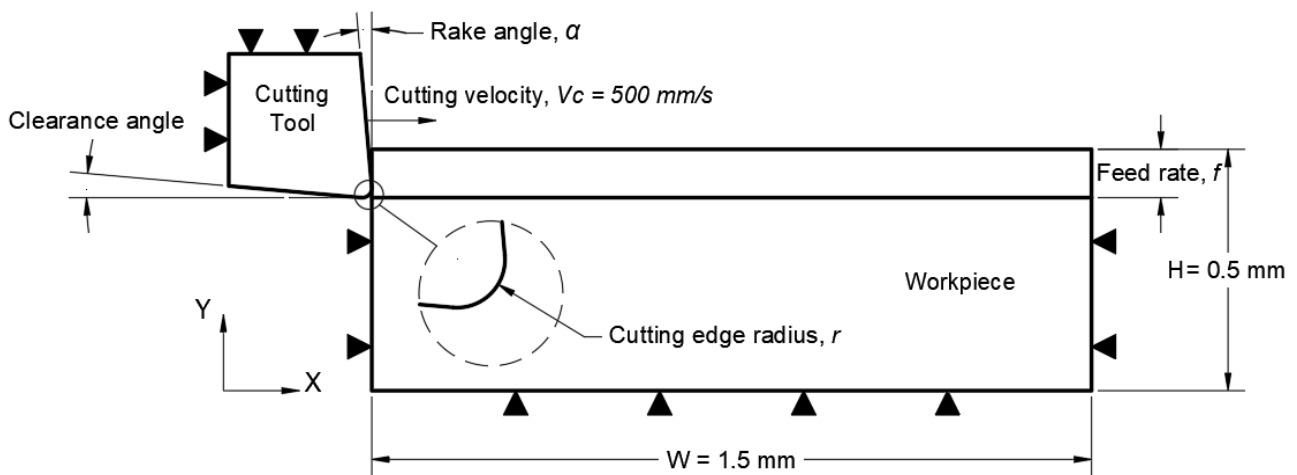

Figure 1 Schematic diagram showing geometry and boundary conditions 2D orthogonal cutting model.

The model is composed of a cutting tool and a workpiece. The workpiece is modeled as a fully constrained rectangular block with a width of 1.5 mm and a height of 0.5 mm. Three different values of undeformed chip thickness (feed rate, f) are adopted: 0.1, 0.2, and 0.3 mm. The depth of cut is assumed constant and equal to 1 mm. The cutting tool has a continuous clearance angle of 5°, three values of rake angle: 5°, 0° and -5° and three values of cutting-edge radius, r: 0.02, 0.04 and 0.06 mm. The cutting tool is constrained in the Y direction and moves in the X direction with a cutting velocity, *Vc,* of 500 mm/s.

The cutting tool and workpiece are meshed using a 4-node bilinear plane strain quadrilateral element with reduced integration (CPE4R). The surface of the cutting tool and the undeformed chip area are meshed with 0.01 mm-sized elements. The workpiece's unmachined area has meshed using 3900 elements with varying mesh sizes ranging between 0.01 to 0.05 mm. The cutting tool

has meshed using 844 elements that ranged in size between 0.01 to 0.024. The mesh strategy is about reducing the computational time with the accepted accuracy of the results. The mesh strategy is composed of the following steps, as mentioned afterward. The mesh size in the cutting zone, the contact face of the cutting tool, and the sacrificial layer are identical. The mesh size in the areas far from the cutting zone is made larger to save computational time. Element size is decided after several trials such that no significant element distortion aborts the computational process. The starting trial to determine the element size was based on the literature review [4, 12] to reduce the number of trials. Mesh refinement is locally applied until the accepted chip serration morphology is produced.

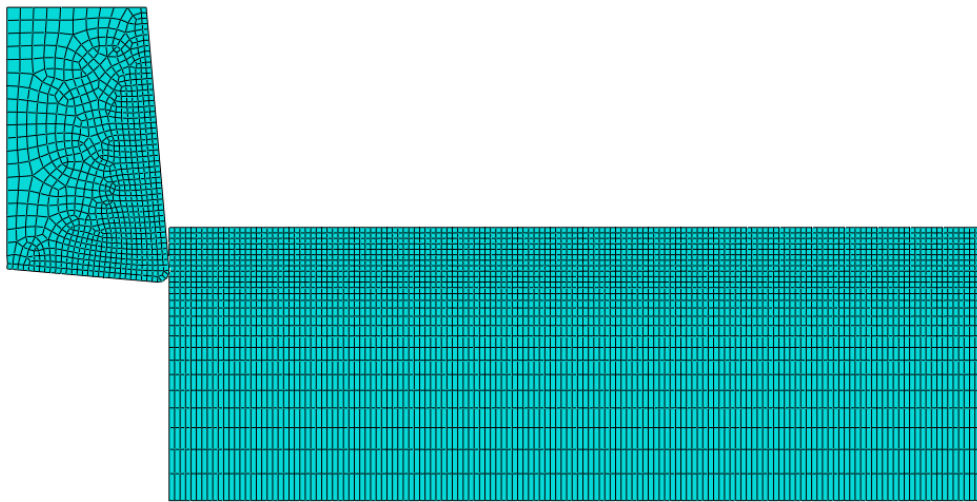Figure 2 shows the mesh topology of the workpiece and the cutting tool.

Figure 2 Workpiece and cutting tool mesh.

The contact model between the cutting tool and the workpiece assumes tangential behavior with a friction coefficient of 0.3 [3] and default normal behavior and heat generation effects.

The workpiece material, Ti6Al4V, is assumed to be homogenous and has an elastic-plastic constitutive response. In contrast, the cutting tool material, Tungsten Carbide (WC), is considered homogenous and perfectly elastic. Table 1 presents the physical properties of the workpiece and the cutting tool [3, 7].

Table 1 Physical properties of the workpiece and the cutting tool.

Physical property	Workpiece material Ti6Al4V [3]	Cutting Tool material WC [7]
Density (tone/mm³)	4.5×10^{-9}	1.19×10^{-8}
Young's modulus (MPa)	144×10^3	534×10^3
Passion's ratio	0.32	0.22
Thermal conductivity (W/m·°C)	6.6	50
Specific heat (mJ/tone·°C)	656×10^6	400×10^6
Expansion coefficient (mm/mm °C)	9.4×10^{-6}	--
Melting temperature (°C)	1660	--

2.2 Workpiece Material Constitutive Model

Johnson-Cook (JC) constitutive model [25] is used to simulate the behavior of Ti6Al4V. JC model is widely used in metal cutting simulations since it accounts for large strains, high strain rates, and temperature effects. The mathematical expression of the JC model is [7]

$$\bar{\sigma} = [A + B\bar{\varepsilon}^n]\left[1 + Cln\left(\frac{\dot{\bar{\varepsilon}}}{\dot{\bar{\varepsilon}}_o}\right)\right]\left[1 - \left(\frac{T - T_r}{T_m - T_r}\right)^m\right] \tag{1}$$

the first term describes elastoplasticity, the second describes viscosity, and the third describes thermal softening. $\bar{\sigma}$ is the equivalent of stress, $\bar{\varepsilon}$ is the equivalent strain, $\dot{\bar{\varepsilon}}$ is the equivalent strain rate, $\dot{\bar{\varepsilon}}_o$ is the reference strain rate, T is the current temperature, T_m is the melting temperature and T_r is the room temperature. A, B, C, n, and m are model coefficients in Table 2 for Ti6Al4V [3].

Table 2 JC model coefficients for Ti6Al4V [3].

A: Initial yield stress (MPa)	870
B: Hardening modulus (MPa)	990
C: Strain rate dependency coefficient	0.011
n: Strain hardening coefficient	0.25
m: Thermal softening coefficient	1
$\dot{\bar{\varepsilon}}_o$	0.7

2.3 Damage Model

Chip separation is simulated using element deletion algorithms provided by ABAQUS, which delete elements with damage values that exceed a critical value. Damage initiation is expressed using the JC shear failure model [4, 26]

$$\varepsilon_{D=0} = [D_1 + D_2 exp(D_3\sigma^*)]\left[1 + D_4 ln\left(\frac{\dot{\bar{\varepsilon}}}{\dot{\bar{\varepsilon}}_o}\right)\right]\left[1 + D_5\left(\frac{T - T_r}{T_m - T_r}\right)\right] \tag{2}$$

where $\varepsilon_{D=0}$ is the equivalent plastic strain at the onset of damage, σ^* is stress triaxiality and equal to $\frac{\sigma_m}{\sigma}$, σ_m is the mean stress, σ is the equivalent Von Mises stress. D_1 to D_5 are model coefficients, and their values for Ti6Al4V are presented in Table 3.

Table 3 JC shear failure model coefficients for Ti6Al4V [3, 5, 7].

D_1	D_2	D_3	D_4	D_5
-0.09	0.25	-0.5	0.014	3.87

Damage accumulation is expressed by

$$w = \sum \frac{\Delta\bar{\varepsilon}}{\varepsilon_{D=0}} \tag{3}$$

where $\Delta\bar{\varepsilon}$ is the increment of plastic strain. At w = 1, damage starts. The behavior of Ti6Al4V during the damage evolution stage is simulated using an energy-based fracture criterion. Gf, also called Hillerborge's fracture energy, is used in this fracture energy model. Fracture energy is the required energy to start a unitary crack and is given by [4]

$$G_f = \int_{\varepsilon_{D=0}}^{\varepsilon_{D=1}} L_c \sigma d\varepsilon = \int_0^{u_{D=1}} \sigma du \tag{4}$$

where L_c is the element's characteristic length, and u is the equivalent displacement. Figure 3 presents material damage evolution and fracture energy.
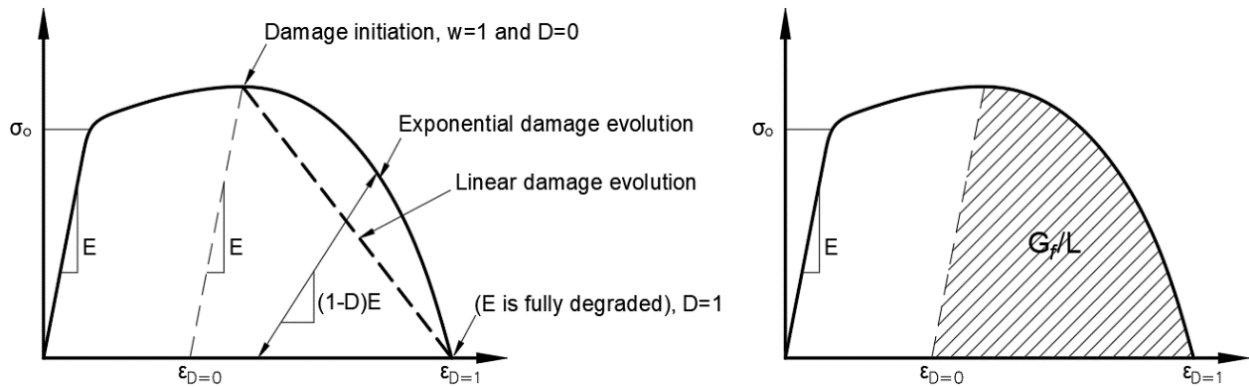

Figure 3 Damage evolution and fracture energy.

Damage starts at u = 0, and the material is considered fully damaged at u = $L_c\varepsilon$. Element geometry controls its characteristic length. In the case of 2D plane conditions, "Lc equals the square root of the element surface" [4]. For the element type (CPE4R), Lc is equal to "half the typical length of a line across a second-order element" [6]. The fracture energy in plane strain conditions can be calculated by [4]

$$G_f = \frac{1 - v^2}{E} K_C^2 \tag{5}$$

where K_c is fracture toughness in mode KIC [4, 27]. Damage evolution, D, is calculated using the exponential relation [4]

$$D = 1 - exp\left(- \int_0^{u_{D=1}} \frac{\sigma}{G_f} du \right) \tag{6}$$

or the linear relation [4]

$$D = \frac{L_c\varepsilon}{u_{D=1}} = \frac{u}{u_{D=1}} \tag{7}$$

Different fracture energy values for Ti6Al4V are found in the literature, namely 33.67 mJ/mm^2 [3] and 18.5 mJ/mm^2 [28]. The energy dissipated during damage evolution is equal to G$_f$ [5].

2.4 Friction Model

The friction between the cutting tool and chip is simulated using a simple shear friction model with shear friction coefficient μ = 0.3 [3].

3. Design of Experiment

Minitab-19 software plans the simulation trials using Taguchi L9 orthogonal array (3 × 3). The goal is to study the effect of rake angle, cutting edge radius, and feed rate on the cutting force and the cutting zone temperature. Table 4 presents the three factors and their levels.

Table 4 Factors and their levels.

Factors	Level 1	Level 2	Level 3
Rake angle, degree	5	0	-5
Cutting edge radius, mm	0.02	0.04	0.06
Feed rate, mm/rev	0.1	0.2	0.3

Nine simulation trials are planned based on different combinations of rake angle, cutting edge radius, and feed rate, see Table 5.

Table 5 Taguchi L9 (3 × 3) layout.

Exp. No.	Rake Angle (deg)	Cutting Edge Radius (mm)	Feed (mm/rev)
1	5	0.02	0.1
2	5	0.04	0.2
3	5	0.06	0.3
4	0	0.02	0.2
5	0	0.04	0.3
6	0	0.06	0.1
7	-5	0.02	0.3
8	-5	0.04	0.1
9	-5	0.06	0.2

4. Results and Discussion

Figure 4 shows cutting force variation with time during orthogonal dry cutting of Ti6Al4V using a WC cutting tool and a cutting velocity of 500 mm/s. It also compares cutting force variation during the machining process using different combinations of cutting tool rake angle, cutting edge radius, and feed rate. It shows that the maximum cutting force occurs in the first stage, which could be related to the first contact between the cutting tool and the workpiece edge. In the second stage, a significant drop in the cutting force occurs due to the formation of the cutting shear zone and the rise of the cutting zone temperature. In the third stage, the cutting force starts increasing gradually

due to serrated chip formation and accumulation on the cutting tool rake surface. Finally, the chip falls and leaves the cutting tool, resulting in the cutting force's drop.
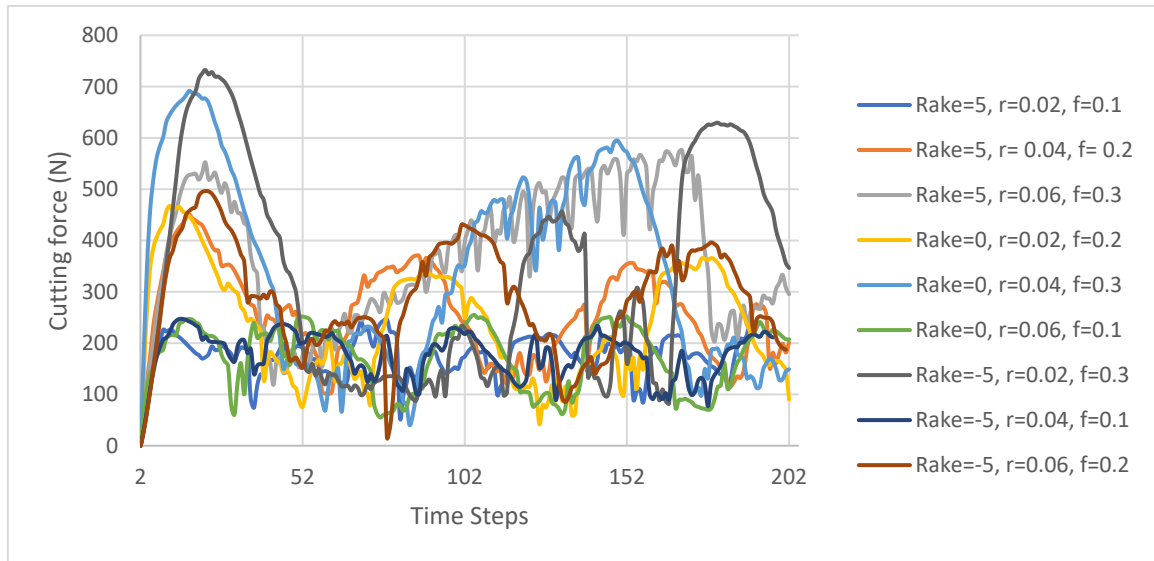

Figure 4 Cutting force variation with time during orthogonal machining of Ti6Al4V at different rake angles, cutting edge radii, and feed rates.

Table 6 presents the average cutting force and average cutting zone temperature from nine numerical simulations. The simulations are based on a constant velocity of 500 mm/min and different combinations of cutting tool rake angles, cutting edge radii, and feed rates. Von Mises stress and temperature distribution in the cutting zone are presented in Figure 5 and Figure 6, respectively. Also, Figure 5 shows chip morphology at selected time steps.

Table 6 Taguchi L9 (3 × 3) experiment combinations for rake angle, cutting edge radius, feed rate, and the responses: average cutting force and cutting zone temperature.

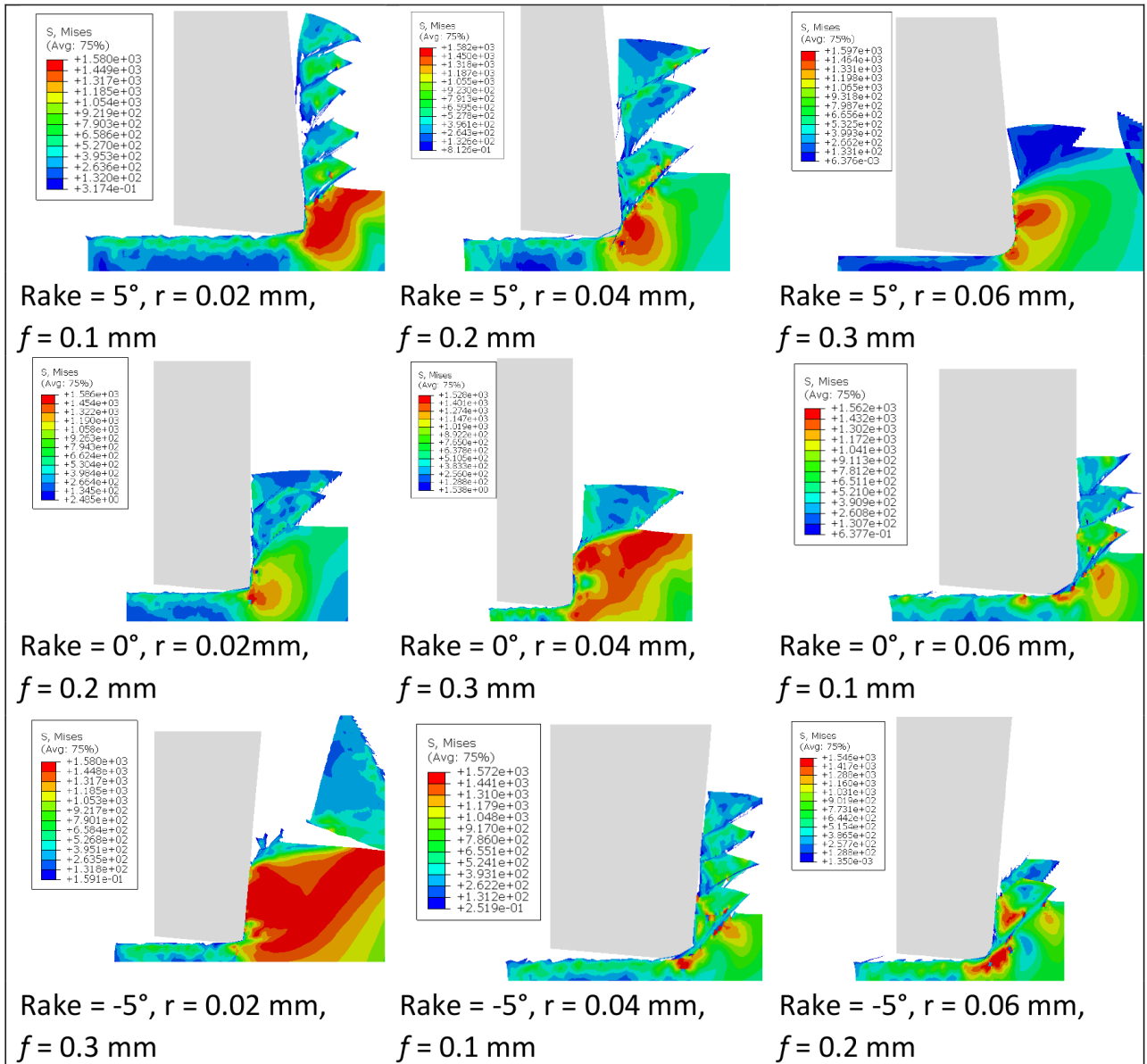| Exp. No.	Rake Angle (deg)	Cutting Edge Radius (mm)	Feed Rate (mm/rev)	Average Cutting Force (N)	Average Cutting Zone Temperature (°C)
1	5	0.02	0.1	175	694
2	5	0.04	0.2	260	741
3	5	0.06	0.3	375	754
4	0	0.02	0.2	238	693
5	0	0.04	0.3	347	699
6	0	0.06	0.1	172	686
7	-5	0.02	0.3	325	688
8	-5	0.04	0.1	178	713
9	-5	0.06	0.2	290	755

Figure 5 Von Mises stresses and chip morphology for the nine experiments at selected time steps.
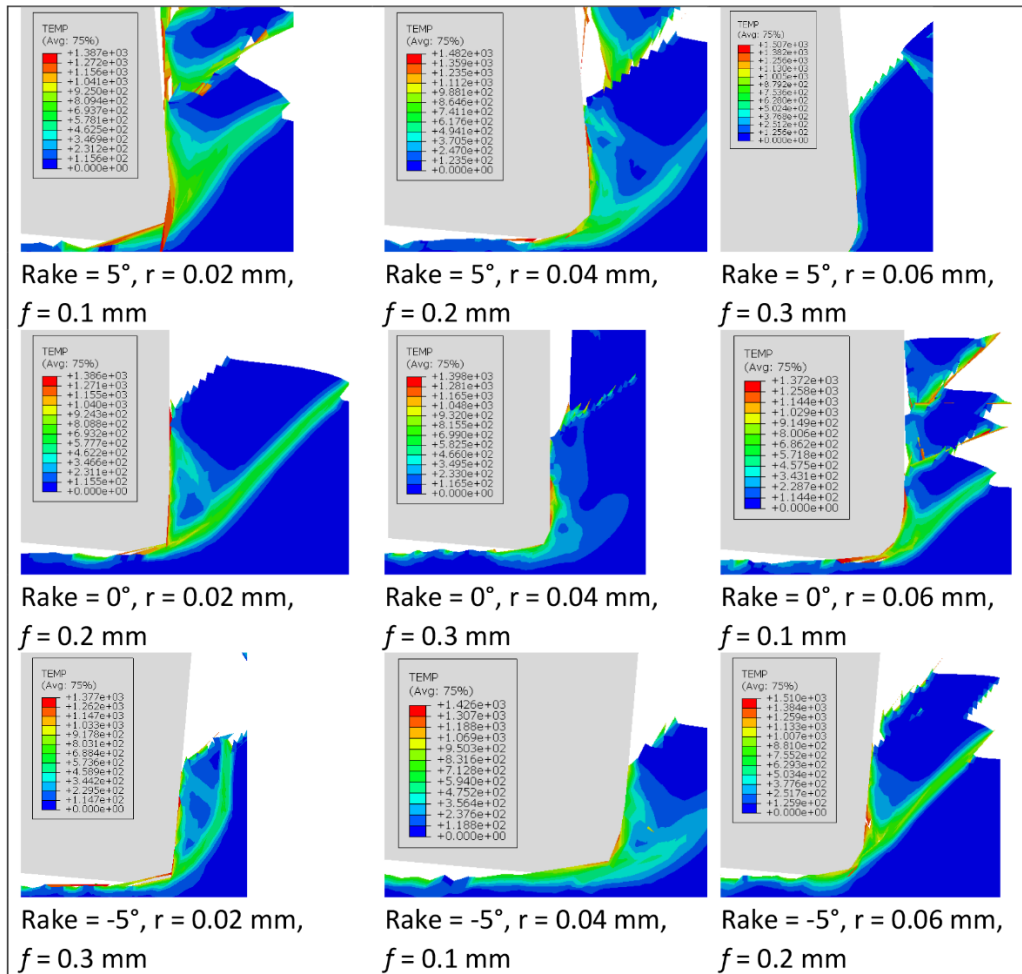
Figure 6 Cutting zone temperature for the nine experiments at selected time steps.

They considered 90% CI, and the ANOVA results in Table 7 show that feed rate has the most significant effect on cutting force, with a high contribution of 94.51%. Rake angle and cutting-edge radius show no significant impact on the cutting force; the total contribution is less than 5%. ANOVA analysis for cutting zone temperature in Table 8 shows that rake angle, cutting edge radius, and feed rate do not significantly affect cutting zone temperature. However, the impact of cutting edge radius has the most enormous contribution to this response with 37.82%, followed by rake angle with a contribution of 33.14% and cutting feed with a contribution of 23.5%. These results must be confirmed by implementing the same study over different factor levels.

Table 7 Analysis of Variance-Cutting force.

Source	DF	Seq SS	Contribution	Adj SS	Adj MS	F-Value	P-Value
Rake angle, deg	2	488.2	1.02%	488.2	244.1	0.95	0.513
Cutting edge radius, mm	2	1634.9	3.40%	1634.9	817.4	3.18	0.239
Feed rate, mm	2	45414.9	94.51%	45414.9	22707.4	88.43	0.011
Error	2	513.6	1.07%	513.6	256.8		
Total	8	48051.6	100.00%				

Table 8 Analysis of Variance – Cutting zone temperature.

Source	DF	Seq SS	Contribution	Adj SS	Adj MS	F-Value	P-Value
Rake angle, deg	2	2166.0	33.14%	2166.0	1083.0	5.98	0.143
Cutting edge radius, mm	2	2472.0	37.82%	2472.0	1236.0	6.83	0.128
Feed rate, mm	2	1536.0	23.50%	1536.0	768.0	4.24	0.191
Error	2	362.0	5.54%	362.0	181.0		
Total	8	6536.0	100.00%				

ANOVA analyses were conducted based on the assumption of normality and equal variance. Kolmogrov-Smirnov (KS) test is used to check normality, while Levene's test is used to check equal variance. Figure 7 and Figure 8 show the Probability Plots for cutting force and cutting zone temperature, respectively. They show that the P value is more significant than 0.05, confirming the normality assumption. Figure 9 shows an example of an equal variance test. Levene's test results are provided in Table 9. The P values for all tests are more excellent than 0.05, which confirms the equal variance assumption.
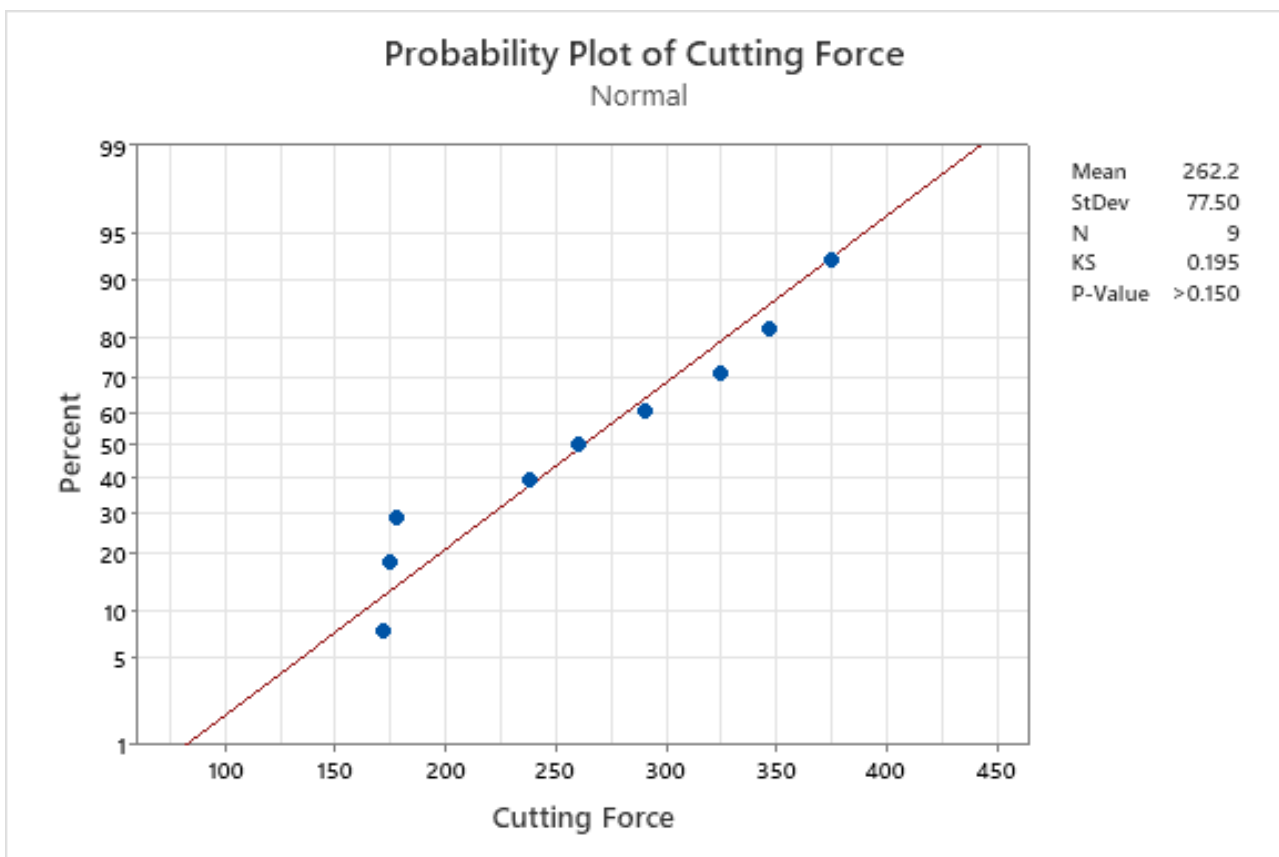

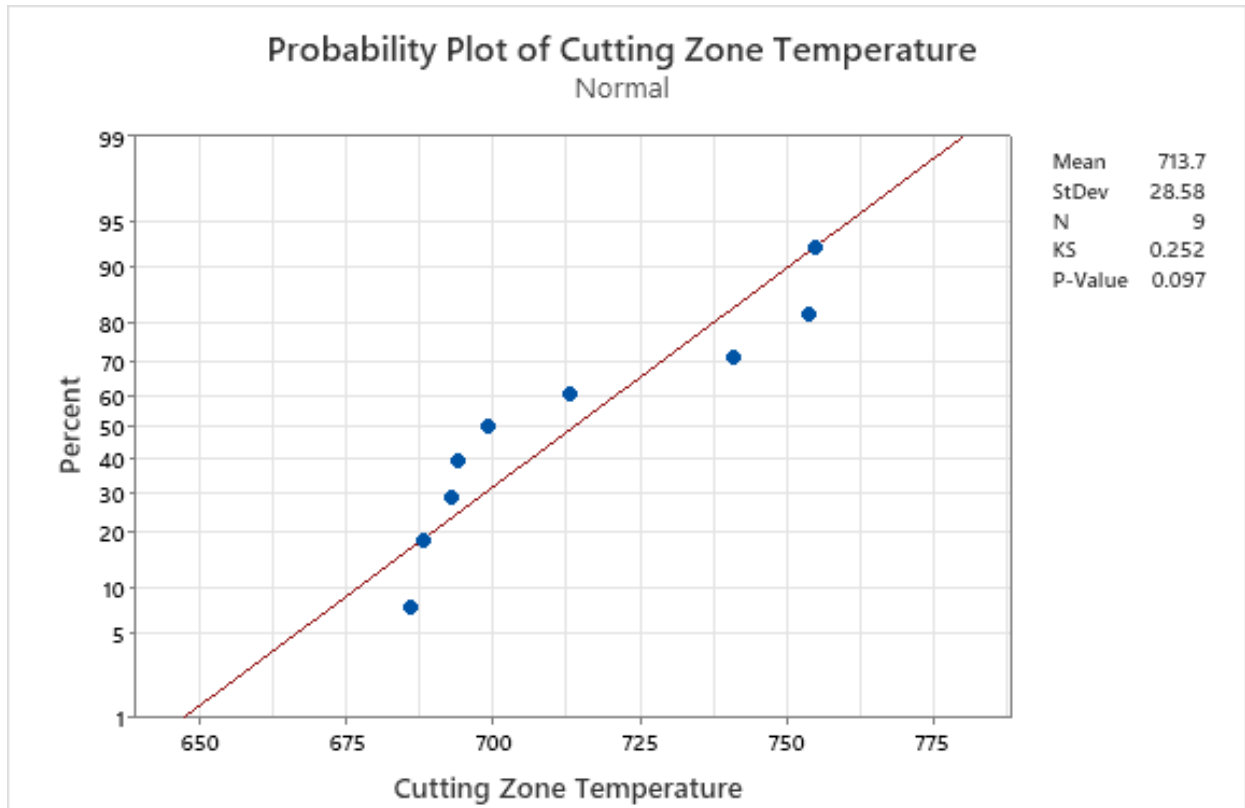**Figure 7** Normality test for cutting force data.

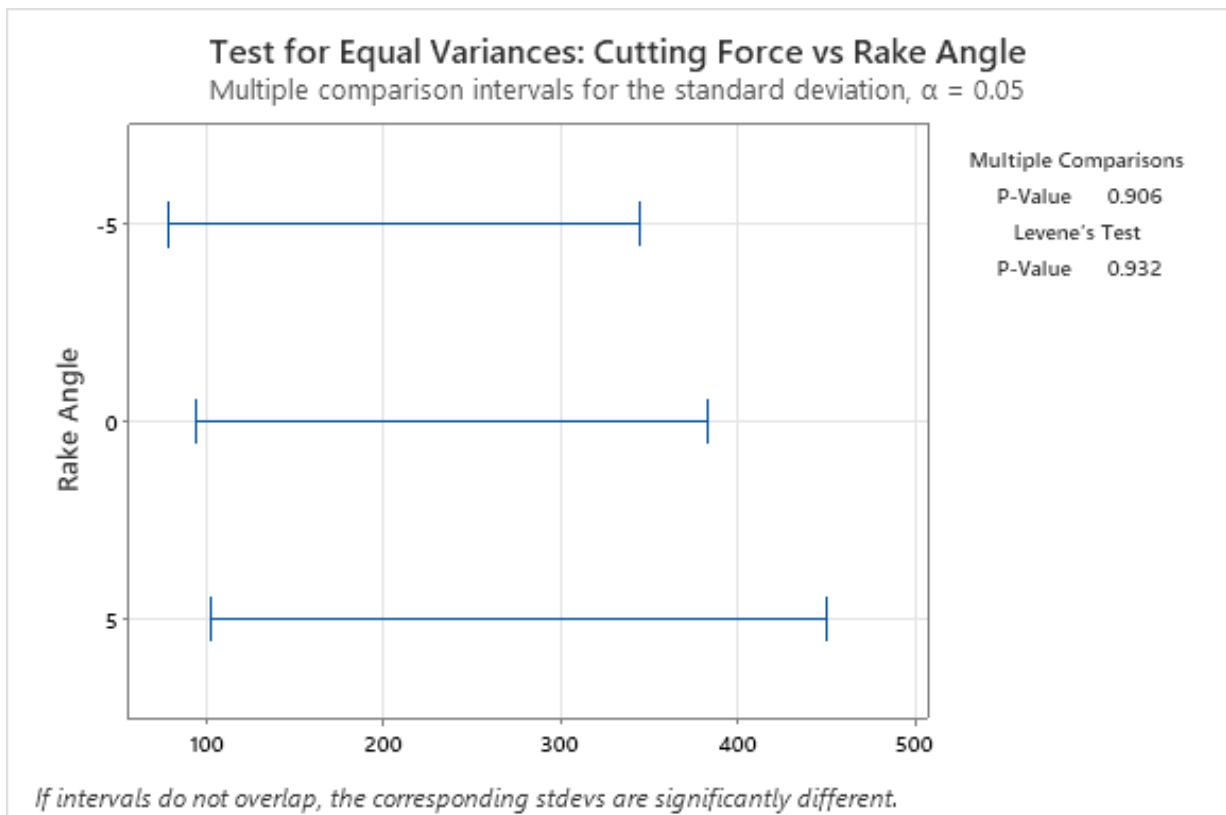**Figure 8** Normality test for cutting zone temperature data.

Figure 9 Equal Variance test for cutting zone temperature data.

Table 9 Equal Variance Tests.

Levene's test	P-value
Cutting Force versus Rake Angle	0.932
Cutting Force versus Cutting Edge Radius	0.916
Cutting Force versus Feed Rate	0.303
Cutting Zone Temperature versus Rake Angle	0.484
Cutting Zone Temperature versus Cutting Edge Radius	0.588
Cutting Zone Temperature versus Feed Rate	0.753

5. Conclusions and Futuristic Work

The effect of cutting tool rake angle, cutting edge radius, and feed rate on the cutting force and cutting zone temperature during orthogonal machining of Ti6Al4V is evaluated using numerical simulation followed by ANOVA. Numerical simulation is a very efficient tool for studying cutting processes because it provides insights into hard-to-measure parameters such as the cutting zone temperature. Chip formation is found to be very sensitive to fracture energy. Although fracture energy is a material property, it's sensitive to element characteristic length. Results showed that only feed rate has a significant effect on cutting force. Rake angle and cutting-edge radius do not significantly impact the cutting force or the cutting zone temperature. This result is valid within the studied factors' used ranges (levels). It is recommended that this study be performed over a broader range of the factors investigated to validate this conclusion.

The study revealed that feed rate was the most dominant input parameter towards the cutting force, and it was found in agreement with the literature. This is because the feed rate is directly linked with the chip load and tends to control the cutting force involved. Rake angle and edge radius were found to be less significant in the case of cutting force. However, regarding the cutting temperature, all input factors were found to have an almost equal contribution.

Finite element analysis is an essential tool that can be engaged to reduce the cost of experimentation and optimize the overall process. The study revealed that manufacturers can use this finite element model to optimize complex geometric parameters such as rake angle and edge radius for machining high-performance materials. In addition, future research can be directed toward developing the digital twin-cutting tool using the finite element model.

Author Contributions

Conceptualization, Mohammed Mustafa, Salman Pervaiz & Ibrahim Deiab; methodology, Mohammed Mustafa.; validation, Mohammed Mustafa; formal analysis, Mohammed Mustafa; investigation, Mohammed Mustafa; resources, Mohammed Mustafa; data curation, Mohammed Mustafa; writing—original draft preparation, Mohammed Mustafa; writing—review and editing, Mohammed Mustafa, Salman Pervaiz & Ibrahim Deiab; supervision, Salman Pervaiz & Ibrahim Deiab; project administration, Salman Pervaiz & Ibrahim Deiab; All authors have read and agreed to the published version of the manuscript.

Competing Interests

The authors have declared that no competing interests exist.

References

1. Jażdżewska M, Kwidzińska DB, Seyda W, Fydrych D, Zieliński A. Mechanical properties and residual stress measurements of grade IV titanium and Ti-6Al-4V and Ti-13Nb-13Zr titanium alloys after laser treatment. Materials. 2021; 14: 6316.
2. Yaich M, Ayed Y, Bouaziz Z, Germain G. Numerical analysis of constitutive coefficients effects on FE simulation of the 2D orthogonal cutting process: Application to the Ti6Al4V. Int J Adv Manuf Technol. 2017; 93: 283-303.
3. Bermudo Gamboa C, Andersson T, Svensson D, Trujillo Vilches FJ, Martín-Béjar S, Sevilla Hurtado L. Modeling of the fracture energy on the finite element simulation in Ti6Al4V alloy machining. Sci Rep. 2021; 11: 18490.
4. Ducobu F, Arrazola PJ, Rivière-Lorphèvre E, Filippi E. On the selection of an empirical material constitutive model for the finite element modeling of Ti6Al4V orthogonal cutting, including the segmented chip formation. Int J Mater Form. 2021; 14: 361-374.
5. Zhang Y, Mabrouki T, Nelias D, Gong Y. FE-model for titanium alloy (Ti-6Al-4V) cutting based on the identification of limiting shear stress at tool-chip interface. Int J Mater Form. 2011; 4: 11-23.
6. Chen G, Ren C, Yang X, Jin X, Guo T. Finite element simulation of high-speed machining of titanium alloy (Ti–6Al–4V) based on ductile failure model. Int J Adv Manuf Technol. 2011; 56: 1027-1038.
7. Wang B, Liu Z. Investigations on the chip formation mechanism and shear localization sensitivity of high-speed machining Ti6Al4V. Int J Adv Manuf Technol. 2014; 75: 1065-1076.
8. Zhen-Bin H, Komanduri R. On a thermomechanical model of shear instability in machining. CIRP Ann. 1995; 44: 69-73.
9. Miguélez MH, Soldani X, Molinari A. Analysis of adiabatic shear banding in orthogonal cutting of Ti alloy. Int J Mech Sci. 2013; 75: 212-222.
10. Selvan MC, Midhunchakkaravarthy D, Senanayake R, Pillai SR, Madara SR. A mathematical modelling of abrasive waterjet machining on Ti-6Al-4V using artificial neural network. Mater Today Proc. 2020; 28: 538-544.
11. Muthuramalingam T, Moiduddin K, Akash R, Krishnan S, Mian SH, Ameen W, et al. Influence of process parameters on dimensional accuracy of machined Titanium (Ti-6Al-4V) alloy in Laser Beam Machining Process. Opt Laser Technol. 2020; 132: 106494.
12. Parida AK, Maity K. Hot machining of Ti–6Al–4V: FE analysis and experimental validation. Sādhanā. 2019; 44: 142.
13. Brehl DA, Dow TA. Review of vibration-assisted machining. Precis Eng. 2008; 32: 153-172.
14. Roy A, Silberschmidt VV. Ultrasonically assisted machining of titanium alloys. In: Machining of titanium alloys. Berlin, Heidelberg: Springer Berlin Heidelberg; 2014. pp. 131-147.
15. Kumar SR, Kulkarni SK. Analysis of hard machining of titanium alloy by Taguchi method. Mater Today Proc. 2017; 4: 10729-10738.
16. Ibrahim GA, Haron CC, Ghani JA. The effect of dry machining on surface integrity of titanium alloy Ti-6Al-4V ELI. J Appl Sci. 2009; 9: 121-127.

17. Sun S, Brandt M, Mo JP. Evolution of tool wear and its effect on cutting forces during dry machining of Ti-6Al-4V alloy. Proc Inst Mech Eng B J Eng Manuf. 2014; 228: 191-202.

18. Rafighi M. The cutting sound effect on the power consumption, surface roughness, and machining force in dry turning of Ti-6Al-4V titanium alloy. Proc Inst Mech Eng C J Mech Eng Sci. 2022; 236: 3041-3057.

19. Hall S, Loukaides E, Newman ST, Shokrani A. Computational and experimental investigation of cutting tool geometry in machining titanium Ti-6Al-4V. Procedia CIRP. 2019; 86: 139-144.

20. Li A, Zang J, Zhao J. Effect of cutting parameters and tool rake angle on the chip formation and adiabatic shear characteristics in machining Ti-6Al-4V titanium alloy. Int J Adv Manuf Technol. 2020; 107: 3077-3091.

21. Pervaiz S, Deiab I, Rashid A, Nicolescu M. Influence of rake angle on the cutting energy when modeling the machining of Ti6Al4V. Proceedings of the 10th International Symposium on Mechatronics and its Applications; 2015 December 08-10; Sharjah, United Arab Emirates. Piscataway: IEEE.

22. Selvakumar SJ, Raj DS. Machinability analysis during finish turning Ti6Al4V with varying cutting edge radius. Mater Manuf Process. 2024; 39: 144-160.

23. Chen G, Caudill J, Chen S, Jawahir IS. Machining-induced surface integrity in titanium alloy Ti-6Al-4V: An investigation of cutting edge radius and cooling/lubricating strategies. J Manuf Process. 2022; 74: 353-364.

24. Chen G, Chen S, Caudill J, Jawahir IS. Effect of cutting edge radius and cooling strategies on surface integrity in orthogonal machining of Ti-6Al-4V alloy. Procedia CIRP. 2019; 82: 148-153.

25. Johnson GR. A constitutive model and data for metals subjected to large strains, high strain rates and high temperatures. Proceedings of the 7th International Symposium on Ballistics; 1983 April 18-21; The Hague, Netherlands. Available from: https://ia800102.us.archive.org/9/items/AConstitutiveModelAndDataForMetals/A%20constitutive%20model%20and%20data%20for%20metals_text.pdf.

26. Johnson GR, Cook WH. Fracture characteristics of three metals subjected to various strains, strain rates, temperatures and pressures. Eng Fract Mech. 1985; 21: 31-48.

27. Henry SD, Dragolich KS, DiMatteo N. Fatigue data book: Light structural alloys. Novelty, OH: ASM International Materials Park; 1995.

28. Cheng W, Outeiro J, Costes JP, M'Saoubi R, Karaouni H, Astakhov V. A constitutive model for Ti6Al4V considering the state of stress and strain rate effects. Mech Mater. 2019; 137: 103103.